Melt-Processable Syndiotactic Polystyrene/Montmorillonite Nanocomposites

Z. M. WANG,[1] T. C. CHUNG,[1] J. W. GILMAN,[2] E. MANIAS[1]

[1]Department of Materials Science and Engineering, Pennsylvania State University, University Park, Pennsylvania 16802

[2]Fire Science Division, Building and Fire Research Laboratory, National Institute of Standards and Technology, Gaithersburg, Maryland 20899

ABSTRACT: Monoalkyl- and dialkyl-imidazolium surfactants were used to prepare organically modified montmorillonites with markedly improved thermal stability in comparison with their alkyl-ammonium equivalents (the decomposition temperatures increased by ca. 100 °C). Such an increase in the thermal stability affords the opportunity to form syndiotactic polystyrene (s-PS)/imidazolium-montmorillonite nanocomposites even under static melt-intercalation conditions in the absence of high shear rates or solvents. Upon nanocomposite formation, s-PS exhibited an improvement in the thermal stability in comparison with neat s-PS, and the β-crystal form of s-PS became dominant. This crystallization response agrees with previous studies of s-PS/pyridinium-montmorillonite hybrids and is tentatively attributed to a heterogeneous nucleation action by the inorganic fillers. © 2003 Wiley Periodicals, Inc.* J Polym Sci Part B: Polym Phys 41: 3173–3187, 2003
Keywords: nanocomposite; syndiotactic polystyrene; montmorillonite; imidazolium

INTRODUCTION

The fact that clays can disperse in organic matrices and polymers has been well established since the 1950s and was a topic of several textbooks in the 1960s and 1970s. However, it was not until the early 1990s, when an industrial group announced a nylon-6/montmorillonite (MMT) composite with impressive material properties,[1] that the research on these polymer/inorganic nano-phase composites was revived and attracted remarkably strong interest. Since then, smectide and synthetic clays have been incorporated as fillers in many engineering and novelty polymers[2] and used in extensive fundamental studies for polymers in confinement and near solid surfaces.[3] From an industrial viewpoint, the dispersion of these ultrathin (1 nm), ultrahigh-surface-area fillers in polymers concurrently improves many of the material properties,[2] that is, the mechanical, thermal, barrier, and solvent resistance, and also provides flame retardancy.[4] From a fundamental scientific viewpoint, intercalated polymers in layered silicates offer well-defined model systems with macroscopic quantities of 1–2-nm-thick confined polymer films.[3]

The dispersion of highly hydrophilic layered silicates (clays or synthetics) in hydrophobic polymers necessitates the exchange of the alkali counterions in the interlayer by organic cationic surfactants. The choice of the organic cationic surfac-

tants is dictated by a balance of entropic and enthalpic factors[5–7] that render the organically modified fillers miscible with given polymers, even under static melt-processing conditions.[8] Typically, alkyl-ammonium surfactants are employed in the vast majority of the current studies and applications, mostly because of the lower cost and the commercial availability of organosilicates based on such surfactants.

Syndiotactic polystyrene (s-PS) has received considerable attention because it is regarded as a new low-cost engineering polymer with various desirable properties, such as high melting temperature (270 °C), fast crystallization rate, low dielectric constant, low permeability to gases, and good chemical resistance. Although the nanocomposite formation of s-PS with organoclays promises to further extend the material properties of the polymer, the fabrication of such nanocomposites by direct melt-intercalation of s-PS into commercial organically treated clays is problematic, mostly because of the thermal degradation of the available organic surfactants (typically alkyl-ammoniums and to a lesser extent phosphoniums), which decompose far below the high temperatures employed for the melt processing of s-PS. The solution casting of s-PS/organo-MMT nanocomposites is definitely possible,[9,10] but the solvents that can be used for s-PS (usually dichlorobenzene or trichlorobenzene) are quite hazardous chemicals. Master-batch approaches, that is, premixing organo-MMT with atactic polystyrene before dispersion in s-PS,[11] yields composites of various dispersions and properties, but with poor reproducibility.[11] Recent approaches employing aromatic cations, such as alkyl-imidazolium[12,13] and alkyl-pyridinium,[14,15] do offer a viable alternative since they can survive much higher temperatures and meet the miscibility requirements for polymer nanocomposite formation.

In this work, we synthesized two alkyl-imidazolium surfactants [1-hexadecyl-imidazolium (Imm-C16) and dihexadecyl-imidazolium (Imm-2C16)] and employed them to form s-PS/organo-MMT nanocomposites by static melt-intercalation. Our objectives are to (1) explore further the imidazoliums, beyond the monoalkyls (i.e., 1-alkyl-2,3-dimethyl-imidazoliums) that have been studied before,[12] because dialkyl-imidazoles offer a wider range of hydrophobicities comparable to those of quaternary amines; (2) prove that sufficiently favorable thermodynamics of mixing exist (i.e., high-shear-rate twin-screw extrusion[14,15] or solvent casting[9,10] are not necessary for forming

s-PS nanocomposites); (3) confirm that the s-PS thermal stability is retained upon composite formation; and (4) elucidate the crystallization behavior of s-PS in the presence of MMT, which is currently a controversial issue.[9,10,14,15]

EXPERIMENTAL

Materials

Na^+-MMT with an exchange capacity of about 0.95 mequiv/g (Na-Cloisite) was obtained from Southern Clay Products, Inc. (TX). Commercially available organically modified MMTs, by octadecyl-ammonium at the cation-exchange capacity (CEC; Nanomer I30E, Nanocor, IL) and by dimethyl-ditallow-ammonium at CEC (Cloisite 20A, Southern Clay Products), were used as received (tallow refers to natural alkyl mixtures consisting mostly of octadecyls and also of smaller fractions of dodecyls, tetradecyls, and hexadecyls[16]). Imidazole (99% pure), 1-iodohexadecane, and tetrahydrofuran (THF) were purchased from Aldrich and used as received.

X-Ray Diffraction (XRD)

XRD data were collected on a Rigaku Geigerflex powder diffractometer with a Dmax-B controller and a vertical goniometer. θ–θ geometry was used. The instrument used radiation from a copper target tube with Cu Kα radiation (λ = 0.1541871 nm).

Transmission Electron Microscopy (TEM)

Ultrathin sections of the s-PS/clay were obtained with an ultramicrotome equipped with a diamond knife. The sections were transferred dry to carbon-coated copper grids (200-mesh). The contrast between the layered silicates and the polymer phase was sufficient for imaging, so no postmicrotoming staining was required. The direct observation of the s-PS/clay nanocomposite structure was realized under bright-field conditions in a JEOL 1200EX operating at 120 kV.

Differential Scanning Calorimetry (DSC)

DSC was performed in a PerkinElmer DSC7 at various heating and cooling rates (5, 10, or 20 °C/min) under a nitrogen atmosphere. To eliminate the influence of the thermal history, we dis-

carded the data from the first heating and cooling cycles and report the data from the second cycles (for both s-PS and s-PS/clay nanocomposites).
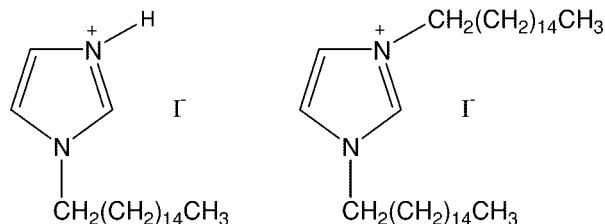
Thermogravimetric Analysis (TGA)

TGA was performed with a PerkinElmer TGA7 instrument under nitrogen at a flow rate of 30 cm^3/min. Before TGA, the samples were carefully purged of air. A scanning rate of 10 °C/min was used, unless stated otherwise. The weight loss rate was also quantified through the derivative of the TGA (DTGA).

Syntheses of the Surfactants, Organoclays, and Nanocomposites

Synthesis of Imm-C16

Imidazole (0.5 g, 7.35×10^{-3} mol) was placed in a 100-mL flask with a reflux condenser; 50 mL of THF was added to the flask to completely dissolve the imidazole. Subsequently, 2.59 g (7.35×10^{-3} mol) of 1-iodohexadecane was added dropwise to the flask with stirring at 55–60 °C. The reactants were left stirring for approximately 12 h. At this point, the complete consumption of imidazole was verified by ^{1}H NMR through the disappearance of the peak at the chemical shift of about 11.8 ppm assigned to the hydrogen connected to the nitrogen of the imidazole ring (Fig. 1). The solution was dried by the removal of THF, and a yellow solid was obtained; this solid was washed three times with 20 mL of hexane. The complete removal of unreacted 1-iodohexadecane was verified by the absence of the peak of 3.28 ppm attributed to CH_2 adjacent to iodium in 1-iodohexadecane. The resultant solid was fully protonated in 30 mL of a hydrochloric acid/methanol solution (1 wt %) for an hour and subsequently dried *in vacuo* to yield a yellow solid. The yield was 2.3 g (74%).

Synthesis of Imm-2C16

The dialkyl-imidazolium was prepared in the same way, only at a higher reaction temperature
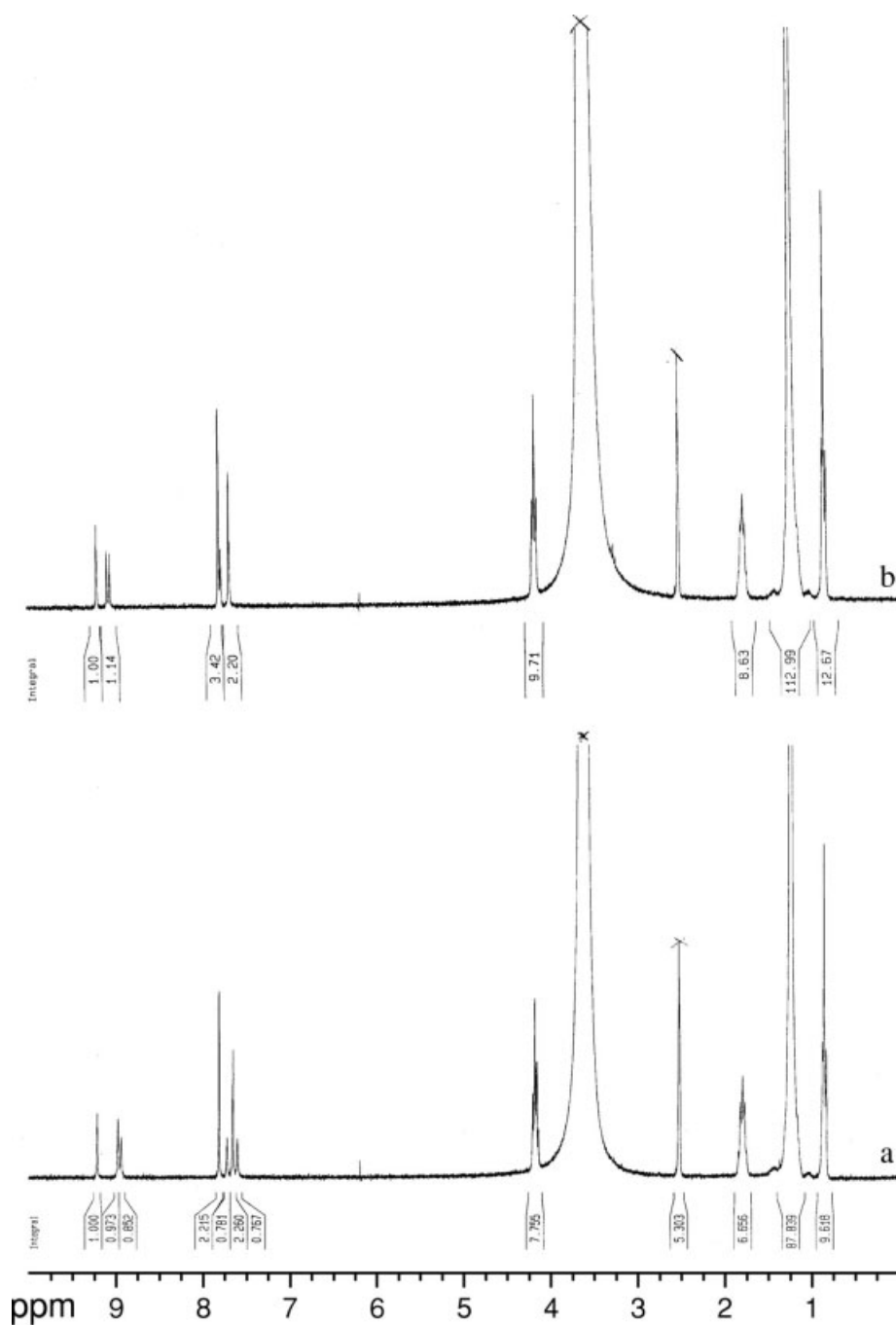
and under an excess of 1-iodohexadecane. Imidazole (0.5 g, 7.35×10^{-3} mol) was dissolved in 50 mL of THF, and 7.77 g (3 times the moles of imidazole) of 1-iodohexadecane was added dropwise to the flask with stirring. The solution was heated to reflux for approximately 48 h at 60–75 °C. After the removal of THF, the resultant purple-yellow solid was washed with large quantities of pentane to remove the unreacted 1-iodohexadecane. The resultant solid was dried *in vacuo* and yielded 2.8 g of the product (34% of yield).
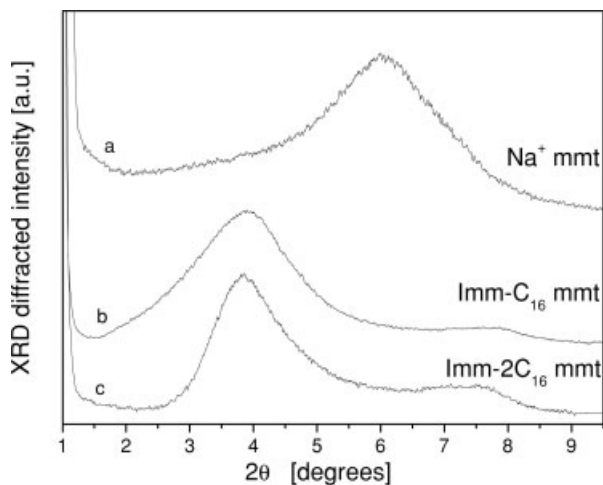
Preparation of the Imidazolium-Modified MMTs

The imidazolium-modified MMTs were synthesized by a cation-exchange reaction of Na^+-MMT and excess imidazolium salt (twice the CEC of MMT). The imidazolium salt (Imm-C16 or Imm-2C16) was dissolved in ethanol at 50 °C and was added to a 1 wt % aqueous suspension of MMT under vivid stirring. The mixture was stirred for 8 h at 50 °C before the imidazolium-exchanged silicates were collected by filtration. The solids were subsequently washed with hot ethanol and paper-filtered three times until an $AgNO_3$ test indicated the absence of halide anions. The filter cake was dried at room temperature, ground, and further dried at 80 °C *in vacuo* for 24 h. The alkyl-imidazolium surfactants differed from those used by Gilman and coworkers[12,13] in studies of amides and poly(ethylene terephthalate) (PET)/imidazolium-MMT nanocomposites. In those studies, two methyl groups were attached to the imidazole ring in the 2- and 3-positions, offering substantially higher hydrophobicity than the present monoalkyl surfactants but more limited opportunities for pending hydrophobic tails than the present dialkyl-imidazoles.

Synthesis of s-PS

The synthesis of s-PS was based on the literature.[17] Toluene (100 mL), 2.61 g (0.045 mol) of methylaluminoxane, and 20.8 g (0.2 mol) of styrene were charged into a flask under an argon atmosphere. After the mixture was stirred for 10 min, 2.5×10^{-5} mol of (cyclopentadienyl) titanium trichloride ($CpTiCl_3$) was added to the mixture. The polymerization reaction proceeded at 50 °C for 2 h and then was stopped at intervals by the addition of 1000 mL of HCl in a methanol solution (1 wt %). The resulting polymer solid was repeatedly washed with 500 mL of methanol and dried at 60 °C *in vacuo* overnight. The chemical

Figure 1. ^{1}H NMR spectra of (a) Imm-C16 and (b) Imm-2C16 surfactants. The chemical shift at 4.20 ppm corresponds to protons from —CH$_2$ connected to the nitrogen of the imidazole ring. The complete disappearance of the peak at 3.21 ppm, attributed to the protons adjacent to iodium, indicates that 1-iodohexadecane has been completely consumed and transferred to imidazolium salts. There are no obvious differences in the chemical shifts of Imm-C16 and Imm-2C16, except for the integral ratio of the protons in the imidazole ring (7.65–9.40 ppm) and of those belonging to alkyl groups (0.90–1.85 ppm).

Figure 2. XRD of (a) Na-MMT and (b,c) the two imidazolium-modified MMTs, Imm-C16-MMT and Imm-2C16-MMT, respectively.

structure of s-PS with [rr] = 99% was verified by ^{13}C NMR.

Preparation of the s-PS-Layered Silicate Nanocomposites

Static melt-intercalation was employed to prepare s-PS/imidazolium-MMT nanocomposites. Namely, an s-PS dried powder and organically treated layered silicate (dried powder, Imm-C16, and Imm-2C16-treated MMT) were mixed and ground together in a mortar and pestle. The mixed powder was heated at 290 °C for 8 h in a vacuum oven. The material was stirred once halfway through the melt-intercalation process.

RESULTS AND DISCUSSION

Characterization of Imidazolium-Modified MMTs

The preparation of the imidazolium-modified MMTs [octadecyl-imidazolium-MMT (Imm-C16-MMT) and dioctadecyl-imidazolium-MMT (Imm-2C16-MMT)] was carried out via standard ion-exchange procedures,[18] as described in the Experimental section. The change in the d-spacing between the silicate layers was measured by XRD. Figure 2 shows that the (001) peak shifts from $2\theta = 6.10°$ to $2\theta = 3.89°$ after modification, indicating a d-spacing increase of 2.27 nm. This larger interlayer spacing is indicative of the larger volume needed in the interlayer gallery to accommodate the cationic surfactants and is sim-
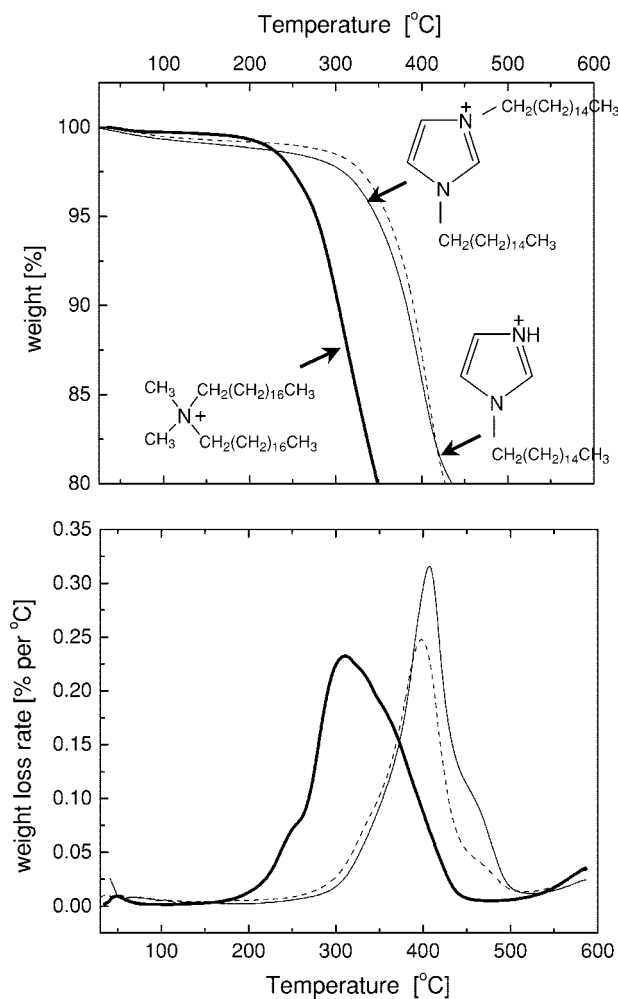
ilar to the d-spacing of MMTs modified by the respective alkyl-ammoniums (C16 and 2C16 alkyls), indicating a surfactant arrangement similar to that in the more common alkyl-ammonium-modified clays.[19]

Thermal Stability of Imidazolium-Modified MMTs

As mentioned previously, improving the thermal stability of the MMT organic treatment is one of the goals of this work. We employed TGA to determine the initial decomposition temperature, the maximum decomposition temperature, and the thermal decomposition activation energy (E_a), also in comparison with an MMT/alkyl-ammonium equivalent. Subsequent XRD offered information on the change of the MMT d-spacing after heat treatment, reflecting the chemical decomposition of the organic surfactants in the interlayer.
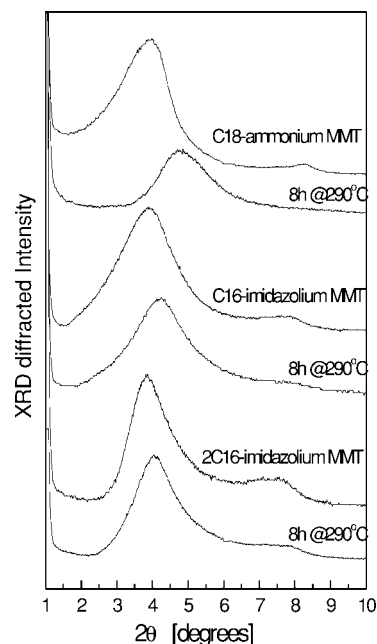
Because of their aromatic ring structure, imidazolium cations have better thermal stability than ammonium cations.[20–22] This behavior is also retained in the presence of MMT; that is, in comparison with alkyl-ammoniums, alkyl-imidazoliums exhibit higher thermal stability when used as organic modifiers for MMT (Fig. 3); the comparison is against a commercial layered silicate, Cloisite 20A, bearing dimethyl-di(hydrogenated tallow)-ammonium surfactants. The TGA data, recorded in a nitrogen atmosphere, are shown in Figure 3, and the respective values are summarized in Table 1. Imidazoliums clearly show a significant improvement in thermal stability in comparison with the alkyl-ammonium equivalent, and in the presence of MMT, they exhibit an onset decomposition temperature and a peak decomposition temperature 100 °C higher than those of ammoniums. Because both cationic surfactants have alkyl hydrophobic tails, this improved temperature stability is directly associated with the better performance of the aromatic imidazoles in comparison with the amine.[12,20] This TGA response demonstrates that these two imidazolium-modified clays may possibly be used for preparing melt-processable polymer/clay nanocomposites with polymers of high softening temperatures, such as amides,[12] PET,[13] and s-PS. Indeed, prolonged heating of alkyl-imidazolium-modified MMTs at elevated temperatures (8 h at 290 °C) shows no trace of surfactant decomposition, whereas the alkyl-ammonium equivalent shows complete removal of the surfactant (Fig. 4).

In agreement with the TGA behavior, XRD also shows that prolonged annealing of organically

Figure 3. (top) TGA and (bottom) DTGA curves for hexadecyl-imidazolium- and dihexadecyl-imidazolium-modified MMT and a commercial di(tallow-alkyl)-ammonium-MMT. All the measurements were carried out at a heating rate of 10 °C/min under nitrogen.

modified MMTs at 290 °C for 8 h *in vacuo* leads to substantial decomposition of the ammonium-based systems in comparison with the imidazo-

Figure 4. Thermal stability of organically modified MMT as reflected in XRD patterns (top) before and (bottom) after heat treatment at 290 °C for 8 h *in vacuo*. From top to bottom, three organo-MMT systems are shown: MMT modified by octadecyl-ammonium (top two patterns), Imm-C16 (middle two patterns), and Imm-2C16 (bottom two patterns).

lium-based ones. For octadecyl-ammonium, the decrease in the interlayer spacing is due to the thermal degradation and desorption of organic materials from within the gallery at high temperatures. Most commonly, such degradation is due to a Hoffman elimination reaction producing an alkene and an amine, leaving a proton in the interlayer; the alkene and amine can easily evaporate from the interlayer gallery, and this results in the shrinkage of the 001 *d*-spacing. In contrast, the imidazolium-treated MMTs show less of a reduction in the *d*-spacing of the layer gallery, as

Table 1. TGA Results for Clays Modified by Imidazolium Salt

Clay Modification	$T_{0.1}$ (°C)	T_{max} (°C)[a]	Char (%)[b]	CEC (mequiv/g)[c]
Imm-C16-MMT	382	398	76 ± 3	1.08 ± 0.18
Imm-2C16-MMT	390	407	72 ± 3	0.76 ± 0.36
Ditallow-ammonium-MMT (Cloisite 20A)	303	299	69 ± 3	0.84 ± 0.36
		366[d]		

[a]Decomposition temperature at the maximum weight-loss rate.
[b]Fraction of the nonvolatile residue.
[c]The CEC as quantified from the mass loss of each sample.
[d]Two peaks are recorded in the DTGA curve for Cloisite 20A.

shown in Figure 4, the (001) peaks for Imm-C16-MMT and Imm-2C16-MMT slightly decrease from $2\theta = 3.90°$ to $2\theta = 4.1°$ and $2\theta = 4.2°$, respectively. This implies that the gallery spacing only decreases by around 0.1 nm for the imidazolium-MMTs, most likely reflecting surfactant rearrangements[18,19] or residual solvent evaporation, rather than thermal decomposition of the alkyl-imidazoliums.

Structure of the s-PS/Clay Nanocomposites

The improved thermal stability of the imidazolium-modified silicates is of key importance in preparing polymer/clay nanocomposites via melt intercalation. However, the organic modification of MMT must also afford favorable thermodynamics for mixing with s-PS, if montmorillonite layers are to be dispersed in the s-PS matrix and nanocomposites are to be formed. The design of our imidazolium hexadecyl and dihexadecyl surfactants was guided by previous studies of atactic polystyrene with layered silicates[5–7,23] because the polymer tacticity is not expected to markedly change the free energy of mixing in these systems. Indeed, the chosen imidazolium surfactants offer sufficient excess enthalpy and promote nanocomposite formation even under the static melt-intercalation conditions employed here (Fig. 5). Both imidazolium-modified MMTs were blended with s-PS at 5 wt % organoclay loading, resulting in an increased interlayer distance of about 3.14 nm, which indicates the development of a miscible s-PS/MMT hybrid structure.

A further evaluation of the composite structure by bright-field TEM (Fig. 5; the darker features correspond to the silicate layers dispersed in the bright s-PS matrix) shows the distribution of clay clusters (tactoids and agglomerates) at a lower magnification and also large numbers of single clay layers dispersed in s-PS at a higher magnification. The MMT layers in parallel registry in the TEM pictures are periodically stacked at about 3–3.5 nm, consistent with the value corresponding to the intercalated XRD peak. In addition, at higher resolution there also exist single inorganic layers with poor parallel registry and wildly varied separation. The presence of well-dispersed/exfoliated MMT layers in the nanocomposite is remarkable, given the static melt-intercalation approach employed to form the nanocomposites, and indicative of the favorable thermodynamics of mixing in the system. Moreover, this approach proves that high-shear-rate process-
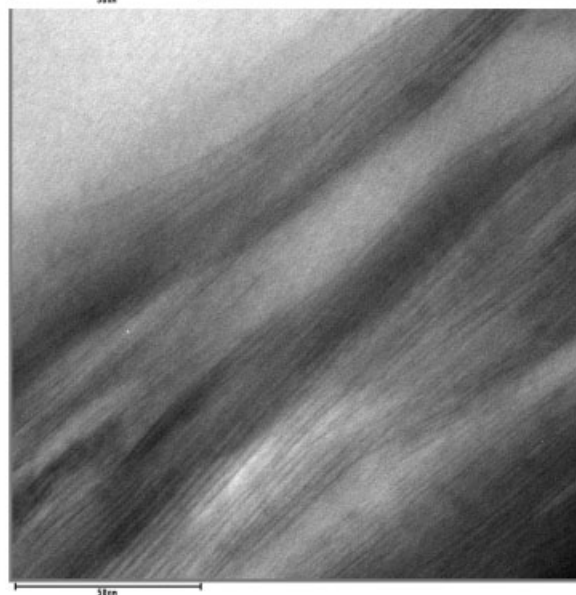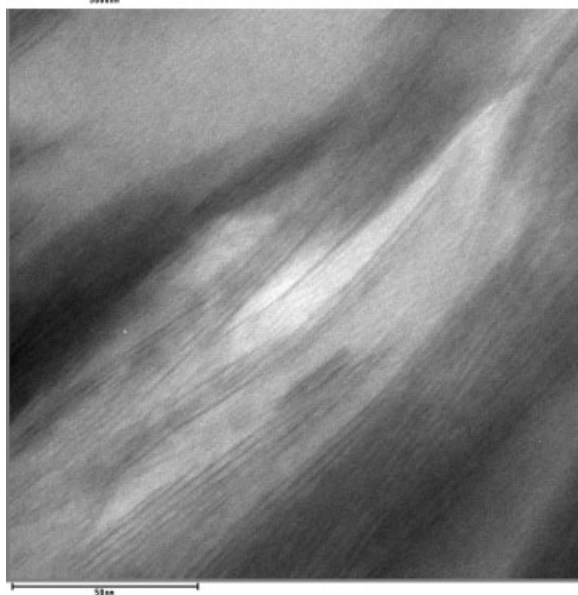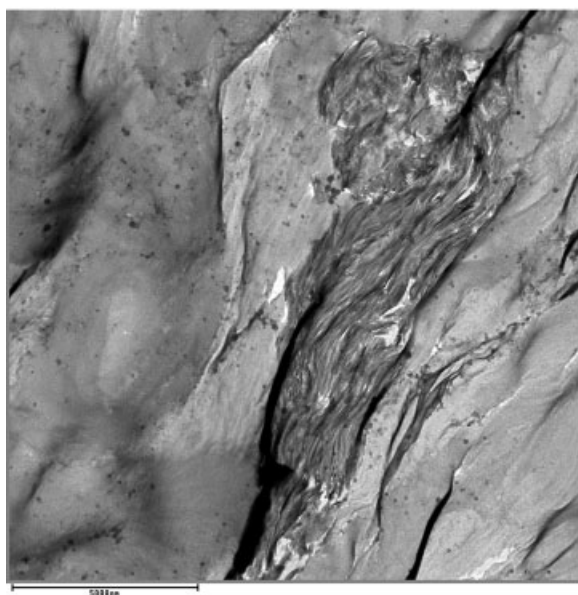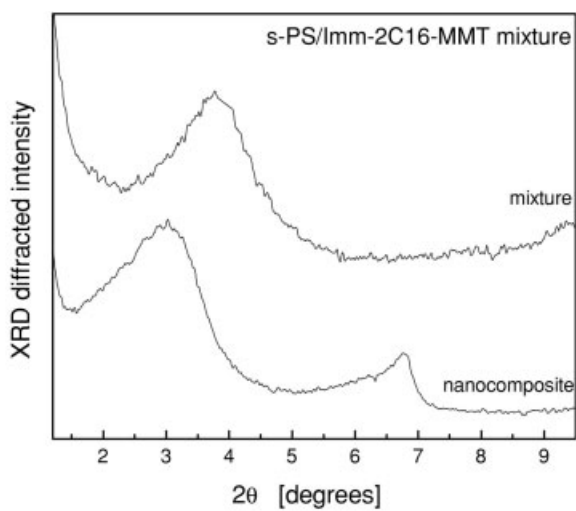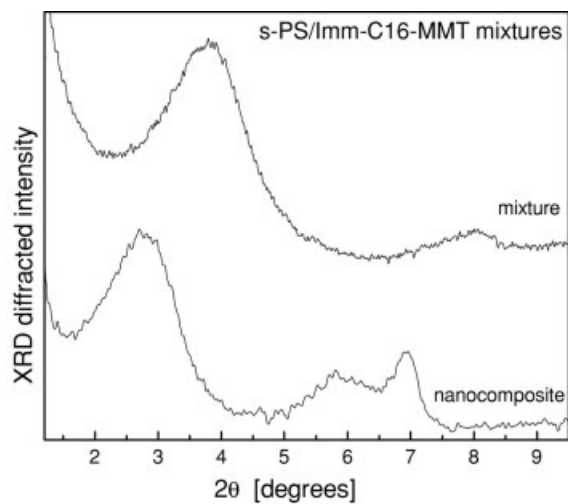
ing, such as twin-screw extrusion, is not necessary for the formation of s-PS/MMT nanocomposites.[13,15]

Thermal Stability of the s-PS/Clay Nanocomposites

The development and research of s-PS is driven by its potential as a low-price engineering material that can endure high temperatures. Obviously, this high thermal stability of s-PS must be retained upon nanocomposite formation if these hybrid composites are to be studied further. The TGA responses under nitrogen for the neat (unfilled) s-PS and its nanocomposites with imidazolium-MMTs are given in Table 2 and Figure 6. As shown by the TGA study, not only do the imidazolium clays not reduce the thermal stability of s-PS, but the s-PS/clay nanocomposites exhibit enhanced thermal stability in comparison with the neat polymer. Table 2 shows the temperature at which 10% degradation occurs ($T_{0.1}$), the temperature at the maximum rate of change of the curve (DTGA), and the presence of shoulders on the derivative curve. The onset temperature of decomposition, measured as $T_{0.1}$, is 20 °C higher for the nanocomposites than for neat s-PS; this behavior is largely maintained throughout the organic decomposition (as shown by the comparable improvement in $T_{0.5}$, the temperature at which 50% degradation occurs). In addition, the DTGA curves of neat s-PS and nanocomposites differ in that a new peak emerges at a higher temperature of about 450 °C for the nanocomposites. Therefore, the nanocomposites exhibit measurable enhanced thermal stability even under a nitrogen atmosphere; as expected,[4] comparable studies under air (in the presence of oxygen) show much higher improvements in the thermal stability with respect to neat s-PS.

Crystallization Behavior of the s-PS/Clay Nanocomposites

s-PS is a fast-crystallizing polymer, and the processing histories can strongly influence its crystal structure and morphologies and, consequently, its properties. It is well established that the crystal forms and processing effects on the polymorphism of s-PS are relatively complicated. The various s-PS crystalline structures are dictated by the chain conformation and the chain packing within the unit cell. According to the nomenclature proposed by Guerra et al.,[24,25] four main crystalline forms can be defined (α, β, γ, and δ). The α and β forms, both containing all-trans planar chains

Table 2. TGA Results for s-PS Hybrids Containing 5 wt % Organo-MMT

Materials	$T_{0.1}$ (°C)[a]	$T_{0.5}$ (°C)[a]	T_{max} (°C)[b]	E_a (kJ mol^{-1})	Char (%)[c]
Neat s-PS	381	414	415	194	0.7
s-PS/Imm-C16-MMT	401	433	424	230	7.2
			452[d]		
s-PS/Imm-2C16-MMT	401	429	425	225	7.7
			450[d]		

[a] $T_{0.1}$ and $T_{0.5}$ correspond to the temperature at 10% and 50% weight loss respectively.
[b] Decomposition temperature at the maximum weight-loss rate.
[c] Amount of the nonvolatile residue measured at the highest temperature.
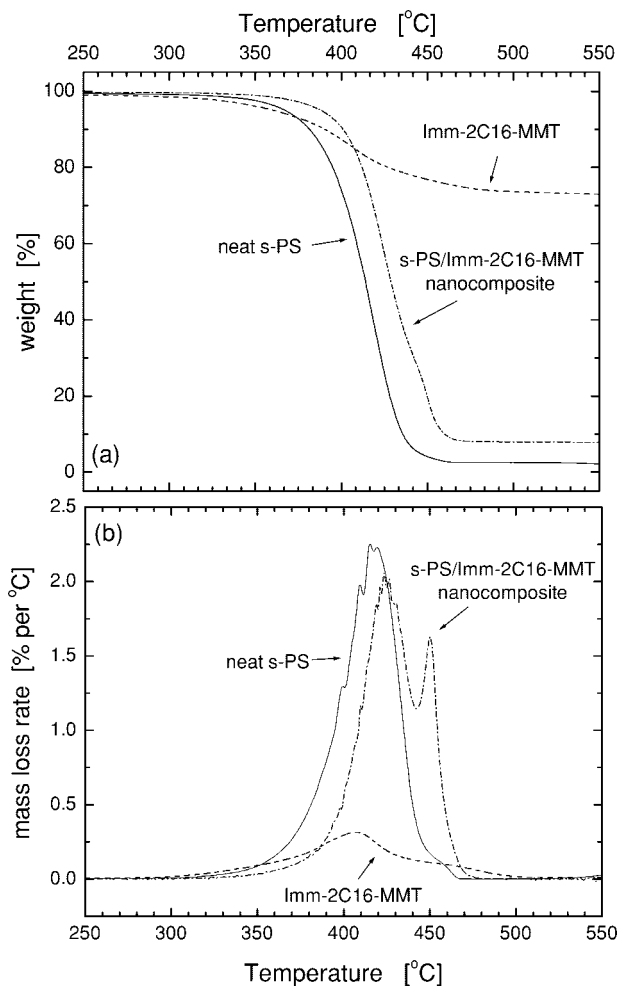[d] Two peaks are measured in the DTGA curves for both s-PS nanocomposites.

with an identity period of c = 0.51 nm, typically result from the melt state of s-PS under different thermal processes, whereas the forms γ and δ, both having (2/1)2 helical chains with an identity period of c = 0.78 nm, are formed under conditions in which solvents are involved. Among these four crystalline forms, the α form with a hexagonal unit cell (a = 2.63 nm) and the β form with an orthorhombic unit cell (a = 0.88 nm and b = 2.88 nm) are more relevant to practical applications because their formation is directly related to standard melt-processing conditions of s-PS. Many techniques, including XRD,[26] electron diffraction,[27] Raman spectroscopy,[28] Fourier transform infrared spectroscopy,[29] and solid-state nuclear magnetic resonance spectroscopy,[30] have been applied to investigate the formation of α- and β-crystalline forms from s-PS, also in the presence of MMT.[13,15]

Upon nanocomposite formation, both the thermal treatment (annealing) and the high-aspect-ratio layered silicates and their extended periodically stacked arrangements can affect the chain conformation and thus the crystalline structure of s-PS.[13,15] Figure 7 shows the XRD patterns for neat s-PS and s-PS/Imm-C16-MMT; for comparison, both the neat polymer and nanocomposite were subjected to the same thermal treatment (annealing at 290 °C *in vacuo* for 2 h, followed by slow cooling to room temperature). The identification of the various diffraction peaks is reported in Tables 3 and 4 and is also compared to the

corresponding theoretical values. Before the thermal treatment, the nascent neat s-PS is dominated by the α-crystal form. After melting at 290 °C for 2 h and cooling down at a rate of about 5 °C/min, most of the α crystal is transformed into the β form, as expected for neat s-PS[13,15] (Fig. 7). In the case of an s-PS/clay system, most of the α-crystal diffraction peaks disappear with the s-PS/clay nanocomposite formation, and the β form dominates in the nanocomposite, as reported before for extruder-mixed cetyl-pyridinium-MMT/s-PS systems.[14,15] Further annealing at 290 °C for 2 h causes no changes in the XRD pattern (Fig. 7). Similar XRD results, while ignoring the neat s-PS polymorphic behavior, have led previous studies to suggest that MMT stabilizes the β-crystal form of s-PS through the development of new pathways for crystal formation.[15]

Such changes in polymer crystallization are not uncommon for polymer/clay nanocomposites and have been reported before in detail for nylon-6[31,32] and poly(vinyl alcohol);[33,34] however, such a stabilization of nonbulk crystal forms in the nanocomposites necessitates the existence of very strong interactions between the inorganic particulates and the polymer [for both nylon and poly(vinyl alcohol), there exist strong hydrogen bonding interactions, which are absent for s-PS[23]]. Thus, despite the similarity in the macroscopic crystallization behavior, those amide and vinyl alcohol systems are qualitatively different from the s-PS/clay systems examined here. Conse-

Figure 5. XRD data and bright-field TEM pictures for the nanocomposite structures. XRD data are shown for the polymer/organoclay physical mixtures before melt intercalation (mixtures) and after static melt-intercalation (nanocomposites). Both alkyl-imidazolium-MMTs, Imm-C16 and Imm-2C16, yielded very similar TEM pictures with a mixed intercalated/exfoliated nanocomposite structure.
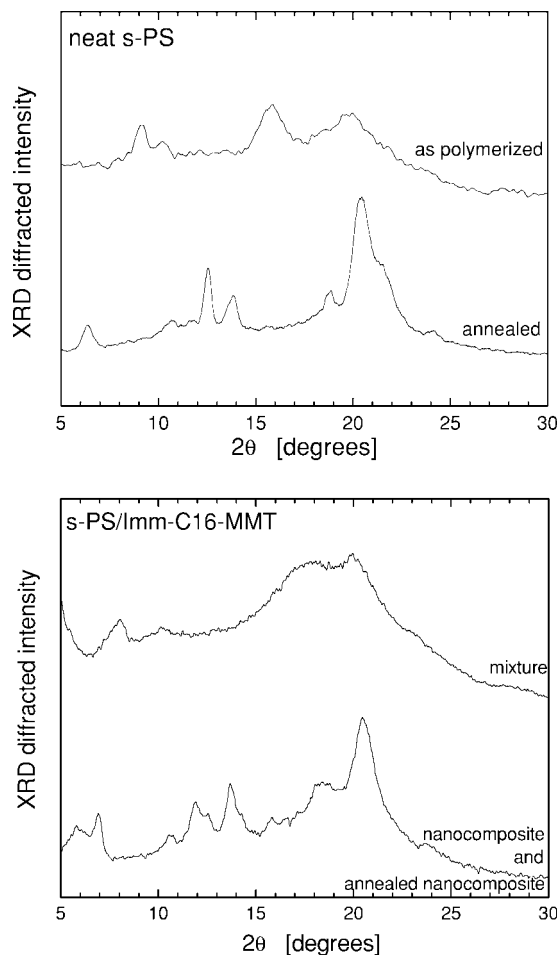
Figure 6. (a) TGA and (b) DTGA curves for neat s-PS, Imm-2C16 modified NMT, and s-PS/Imm-2C16-MMT nanocomposite hybrid. All TGAs were run under nitrogen at 10 °C/min.

quently, this leads us to postulate that the dominance of the β-crystal form in the s-PS/MMT nanocomposites is simply the result of the high processing temperatures needed for the melt blending of the nanocomposites; exposing the bulk (unfilled) s-PS to similar high temperatures also promotes the β-crystal form in s-PS free of MMT. At the same time, the survival of a detectable α crystal in the nanocomposite strongly indicates that MMT stabilizes this α-crystal form at the expense of the β form, as reported in previous studies,[9] and despite the extended annealing at high temperatures during the melt intercalation and the subsequent melt crystallization.

For melt-crystallized s-PS systems studied by DSC, three distinct melting peaks are typically observed (Fig. 8). Although there is no universal

agreement on the assignment of these melting peaks, current opinion attributes peaks 1 and 3 to the β-crystal form, whereas peak 2 is associated with the melting of the α crystal.[35,36] In addition, if neat s-PS is held (melt-crystallized) at a certain temperature for a sufficient time before it is scanned, only two peaks or even a single peak may be observed. During melt-crystallization from high temperatures, the β crystal is the thermodynamically preferred way of molecular packing, whereas the α crystal is suggested to be an alternative kinetic mechanism of packing for s-PS

Figure 7. (top) XRD of the neat s-PS as polymerized and after melt crystallization at 290 °C for 2 h (annealed). (bottom) XRD of s-PS/Imm-C16-MMT before melt intercalation (mixture) and after melt intercalation 8 h at 290 °C (nanocomposite). Subsequent annealing of the nanocomposite for 2 h at 290 °C does not change the XRD pattern. The diffraction angle scale is focused on the 9.5–30° range, within which the most important of the s-PS crystalline peaks appear. The crystallographic identification of the XRD reflections in the diffraction patterns is listed in Tables 3 and 4.

Table 3. XRD Identification for Neat s-PS

Before Annealing					After Annealing (290 °C for 2 h)				
2θ (°)	d (Å)	s-PS Form	hkl	d_{theo} (Å)[a]	2θ (°)	d (Å)	s-PS Form	hkl	d_{theo} (Å)[a]
10.24	8.64	α	210	8.60	6.33	13.96	β	020	14.40
11.71	7.56	α	300	7.58	10.65	8.31	β	110	8.42
15.79	5.61	α	400	5.68	11.71	7.56	α	300	7.52
20.20	4.47	α	211	4.35	12.60	7.03	β	040	7.20
		and β	111	4.34	13.83	6.40	β	130	6.49
					18.73	4.74	β	060	4.80
					20.44	4.35	β	111	4.34
							and α	211	4.35
					21.50	4.13	β	041	4.14
					24.11	3.69	β	080	3.60

[a]d-Spacing of hkl for a perfect crystal form (α or β).

chains with reduced molecular mobility within partially solidified s-PS[35] (and thus promoted for lower crystallization/annealing temperatures).
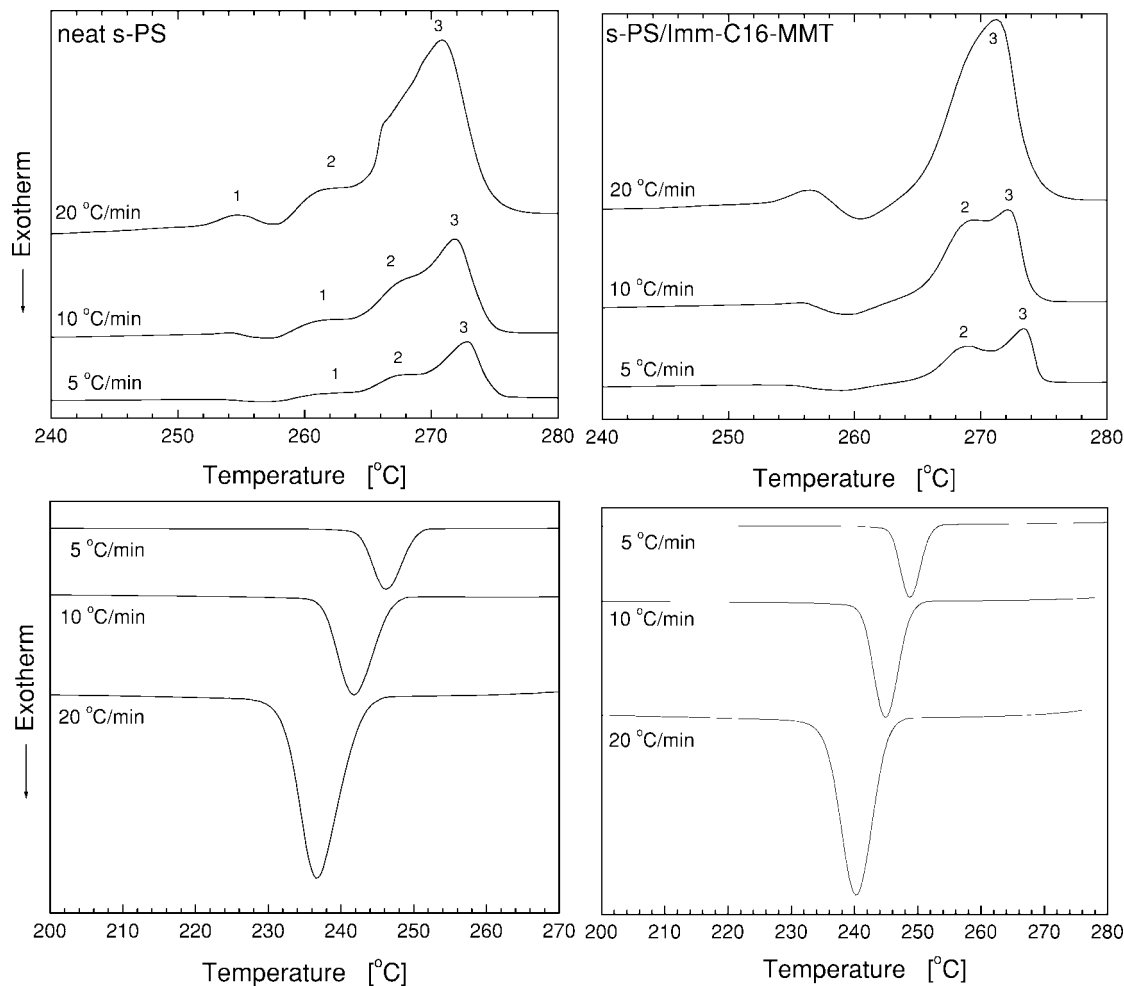
Figure 8 shows the DSC traces for neat s-PS and the corresponding s-PS/Imm-C16-MMT nanocomposite at three different heating and cooling rates. Regardless of the heating rate, three melting peaks are detected for neat s-PS, whereas for the s-PS/clay nanocomposite, only two melting peaks are clearly observed at heating rates of 5 and 10 °C/min (Table 5 summarizes the results of these melting peaks; given the asymmetry of the DSC melting peaks, standard peak fitting can identify peaks 2 and 3 and can detect

the existence of a very weak peak 1). Following the current opinion, melting peaks 1 and 3 correspond to the melting of thin and thick β-crystal lamellae, respectively. A portion of the β crystal reorganizes into thick lamellae during further crystallization, and the remainder of the crystallized s-PS reorganizes as thin lamellae.[36,37] In comparison with neat s-PS, s-PS/clay nanocomposites have a slightly higher melting temperature, regardless of the crystal form and the absence of peak 1, as well as an increased intensity of peak 2. This behavior has been attributed to the role of clay as a nucleating site for the heterophase crystallization of s-PS.[15] This

Table 4. XRD Identification for the s-PS-Imm-C16-MMT Mixture and Nanocomposite

Mixture					Nanocomposite				
2θ (°)	d (Å)	s-PS Form	hkl	d_{theo} (Å)[a]	2θ (°)	d (Å)	s-PS Form	hkl	d_{theo} (Å)[a]
3.75	23.56	clay	001	—	2.81	31.44	clay	001	—
8.00	11.05	α	200	11.37	6.10	14.49	β	020	14.40
10.30	8.59	α	210	8.59	6.87	12.87	α	110	6.73
17.90	4.96	α	410	4.96	10.63	8.32	β	110	8.42
20.10	4.42	α	211	4.35	11.93	7.42	β	120	7.52
		and β	111	4.34	12.50	7.08	β	040	7.20
					13.69	6.47	β	130	6.49
					15.80	5.61	β	140	5.58
					18.12	4.90	α	410	4.96
					20.42	4.35	β	111	4.34
							and α	211	4.35
					23.79	3.74	β	170	3.73

[a] d-Spacing of hkl for a perfect crystal form (α or β).

Figure 8. DSC traces for (left) neat s-PS and (right) the s-PS/Imm-C16-MMT nanocomposite upon (top) heating and (bottom) cooling for three different heating and cooling rates.

explanation is also in concert with the fact that in the presence of MMT the number of initial nuclei tends to increase markedly during melt crystallization, with a concurrent decrease in the crystallite size.[38] This decrease in the crystallite size is generally seen in polymer/clay nanocomposites, across different semicrystalline polymers [e.g., nylon-6, polypropylene, poly(ethylene oxide) (PEO), and poly(vinyl alcohol)[31–34,38–41]], and independently of whether MMT stabilizes a different crystal form,[31–34] amorphizes the polymer,[41] or simply acts as a heterogeneous nucleation site.[39]

Finally, the hypothesis that MMT is acting as a heterogeneous nucleation agent is also supported by the cooling traces of the DSC experiments (Fig. 8). Namely, upon cooling, the crystallization temperatures (T_c's) of the s-PS/clay nanocomposite are systematically higher (by ca. 3 °C; Table 5) than those of neat s-PS at the same cooling rate. The insensitivity of ΔT_c (the difference between T_c of neat s-PS and T_c of its nanocomposite) to the cooling rate indicates that the shift in T_c is not due to any change in the thermal conductivity caused by the addition of the inorganic fillers; in this latter case, ΔT_c would have been a strong function of the cooling rate. Attributing this increase in T_c to a heterogeneous nucleation action of MMT can only be done tentatively on the basis of the reported data (the enumeration of the half-times of crystallization is necessary to definitively illustrate such a viewpoint), and we refer the interested reader to detailed previous studies of similar systems.[15]

Table 5. Comparison of the DSC Measured Melting Temperatures and T_c's for Neat (Unfilled) s-PS and Its Nanocomposite with 5 wt % Imm-C16-MMT at Various Heating and Cooling Rates

Heating Rate (°C/min)	Peak	Crystal Form	Melting Temperature (°C)	
			Neat s-PS	s-PS/Imm-C16-MMT Nanocomposite
5	1	β	261.4	Weak
	2	α	267.8	269.1
	3	β	272.8	273.4
10	1	β	260.9	Weak
	2	α	267.8	269.5
	3	β	271.8	272.2
20	1	β	254.8	257.0
	2	α	262.4	268.5
	3	β	270.8	271.2

Cooling Rate (°C/min)	T_c (°C)		ΔT_c (°C)
	Neat s-PS	s-PS/Imm-C16-MMT Nanocomposite	
5	246.2	248.8	2.6
10	241.7	244.9	3.2
20	236.6	240.2	3.4

CONCLUSIONS

Two imidazolium surfactants (hexadecyl and dihexadecyl imidazolium) were synthesized and successfully used to prepare organically modified MMTs with markedly improved thermal stability in comparison with their alkyl-ammonium equivalents. TGA data show that the onset and maximum decomposition temperatures of the imidazolium-modified MMTs are 100 °C higher than those of alkyl-ammonium clays. Such an increase in the thermal stability affords the opportunity to form s-PS/imidazolium-MMT nanocomposites even under static melt-intercalation conditions, with a slight improvement (by ca. 20 °C) in the s-PS thermal stability compared with that of neat s-PS. Finally, upon nanocomposite formation, the β-crystal form of s-PS becomes dominant; this response agrees with previous studies of s-PS/pyridinium-MMT hybrids and is tentatively attributed to a heterogeneous nucleation action by the inorganic fillers.

APPENDIX

In our endeavor to develop synthetic routes for s-PS/MMT nanocomposites, we have also developed two more methods[38] based on functionalized s-PS. Namely, functionalized s-PS random copolymer (s-PS-OH) can be melt-blended with high-temperature organo-MMTs, whereas s-PS-*block*-PEO copolymers can disperse pristine Na^+-MMT when cast from a solution.

s-PS-OH/Imidazolium-MMT Nanocomposite

The functionalized random s-PS copolymer s-PS-*random*-styrene-*para*-$(CH_2)_4$-$OH^{[42]}$ differs from neat s-PS in that the former shows a slightly lower melting point and better processability, as well as improved affinity to the silicon oxide surfaces of MMT. We used s-PS-OH with 2.1 mol % OH-containing comonomer and Imm-2C16-MMT to prepare the s-PS/clay nanocomposite via a static melting process at 280 °C for 2 h. The XRD

Figure A1. Feasibility of alternate routes for the synthesis of s-PS/MMT nanocomposites as demonstrated by XRD. On the left the XRD patterns of s-PS-OH melt-blended with hexadecyl-imidazolium-MMT before annealing (mixture) and after static melt-intercalation at 280 °C (nanocomposite). On the right the XRD patterns of the s-PS/PEO block copolymer and Na$^+$-MMT physical mixture (mixture) and nanocomposite as cast from solution (nanocomposite).

results show that the (001) peak of the clay shifts from $2\theta = 3.89$ to $2\theta = 2.71°$; that is, the d-spacing increases from 2.27 to 3.15 nm. This indicates that the s-PS-OH/clay nanocomposite definitely forms a miscible nanocomposite; preliminary TEM studies also show a substantial number of exfoliated MMT layers. Therefore, the use of s-PS-OH for preparing the s-PS/clay nanocomposite can further benefit from milder processing conditions, including a lower processing temperature and a shorter processing time, and can lead to highly dispersed MMT in the s-PS matrix.

s-PS-*block*-PEO Copolymer/Na$^+$-MMT Nanocomposite

Because of their favorable interactions with pristine silicate surfaces, PEO blocks can mediate the dispersion of hydrophobic polymers in MMT by replacing the water from within the MMT layers and coordinating to the native cations (Na$^+$, Li$^+$, etc.). Typically, for block copolymers, very short blocks[39] are necessary for this approach to form polymer/clay nanocomposites [e.g., 5 mol % for PP-*b*-PMMA (weight-average molecular weight = 1.5 × 10^4 g/mol) and 3 mol % for PP-*b*-PEO (weight-average molecular weight = 2 × 10^5 g/mol)], and consequently the crystallinity and melting point of the polymer are not affected. Here however, it may be beneficial to have a longer PEO block in s-PS so as to reduce the melt-processing temper-

ature of the polymer and also increase the hydrophilicity (and thus the affinity to Na$^+$-MMT); therefore, in this approach we used s-PS-*b*-PEO (s-PS block, number-average molecular weight = 110 × 10^3 g/mol with 25 mol % PEO block, number-average molecular weight ∼ 8 × 10^3 g/mol) and sodium-MMT to prepare an s-PS/clay nanocomposite cast from a trichlorobenzene/water solution. Figure A1 shows that the (001) peak of MMT shifts from $2\theta = 7.05$ to $2\theta = 4.86°$ (i.e., the d-spacing increases from 12.5 to 18.2 nm), indicating the intercalated structure formed in the s-PS/clay nanocomposite. DSC curves show that the crystallinity and melting temperature of the s-PS block in the nanocomposite do not change in comparison with those of the neat polymer. Therefore, using a functional diblock copolymer may be an effective alternative for preparing polymer/clay nanocomposites without the use of organic cationic surfactants.

REFERENCES AND NOTES

1. Kojima, Y.; Usuki, A.; Kawasumi, M.; Okada, A.; Fukushima, Y.; Kurauchi, T.; Kamigaito, O. J Mater Res 1993, 8, 1185.
2. Alexandre, M.; Dubois, P. Mater Sci Eng 2000, 28, 1.
3. Giannelis, E. P.; Krishnamoorti, R. K.; Manias, E. Adv Polym Sci 1998, 138, 107.

4. Gilman, J. W.; Jackson, C. L.; Morgan, A. B.; Harris, R.; Manias, E.; Giannelis, E. P.; Wuthenow, M.; Hilton, D.; Philips, S. H. Chem Mater 2000, 45, 1866.

5. Vaia, R. A.; Giannelis, E. P. Macromolecules 1997, 30, 7090.

6. Vaia, R. A.; Giannelis, E. P. Macromolecules 1997, 30, 8000.

7. Balazs, A. C.; Singh, C.; Zhulina, E. Macromolecules 1998, 31, 8370.

8. Vaia, R. A.; Ishii, H.; Giannelis, E. P. Chem Mater 1993, 5, 1694.

9. Wu, T.-M.; Hsu, S.-F.; Wu, J.-Y. J Polym Sci Part B: Polym Phys 2002, 40, 736.

10. Wu, H. D.; Tseng, C. R.; Chang, F. C. Macromolecules 2001, 34, 2992.

11. Park, C. I.; Park, O. O.; Lim, J. G.; Kim, H. J. Polymer 2001, 42, 7465.

12. Gilman, J. W.; Awad, W. H.; Davis, R. D.; Awad, W. H.; Davis, R. D.; Shields, J.; Harris, R. H.; Davis, C.; Morgan, A. B.; Sutto, T. E.; Callahan, J.; Trulove, P. C.; DeLong, H. C. Chem Mater 2002, 14, 3776.

13. Davis, C. H.; Mathias, L. J.; Gilman, J. W.; Schiraldi, D. A.; Shields, J. R.; Trulove, P.; Sutto, T. E.; Delong, H. C. J Polym Sci Part B: Polym Phys 2002, 40, 2661.

14. Wu, H. D.; Tseng, C. R.; Chang, F. C. J Appl Polym Sci 2002, 86, 2492.

15. Wu, T.-M.; Hsu, S.-F.; Wu, J.-Y. J Polym Sci Part B: Polym Phys 2003, 41, 560.

16. Hanley, H. J. M.; Muzny, C. D.; Ho, D. L.; Glinka, C. J.; Manias, E. Int J Thermophys 2001, 22, 1435.

17. Ishihara, N.; Kuramoto, M.; Uoi, M. Macromolecules 1988, 21, 3356.

18. Vaia, R. A.; Teukolsky, R. K.; Giannelis, E. P. Chem Mater 1994, 6, 1017.

19. Hackett, E.; Manias, E.; Giannelis, E. P. J Chem Phys 1998, 108, 7410.

20. Hofmann, K. Imidazole and Derivatives; Interscience: New York, 1953; Part 1.

21. Wilkes, J. S.; Lavesky, J. A.; Wilson, R. A.; Hussey, C. L. Inorg Chem 1982, 21, 1263.

22. Ngo, H. L.; LeCompte, K.; Hargens, L.; McEwen, A. B. Thermochim Acta 2000, 97, 357.

23. Manias, E.; Chen, H.; Krishnamoorti, R. K.; Genzer, J.; Kramer, E. J.; Giannelis, E. P. Macromolecules 2000, 33, 7955.

24. Guerra, G.; Vitagliano, V. M.; De Rosa, C.; Petraccone, V.; Corradini, P. Macromolecules 1990, 23, 1539.

25. Guerra, G.; De Rosa, C.; Vitagliano, V. M.; Petraccone, V.; Corradini, P. J Polym Sci Part B: Polym Phys 1991, 29, 265.

26. Vittoria, V.; Russo, R.; De Candia, F. J. Macromol Sci Phys 1989, 28, 419.

27. Pradere, P.; Thomas, E. L. Macromolecules 1990, 23, 4954.

28. Kellar, E. J. C.; Evans, A. M.; Knowles, J.; Galiotis, C.; Andrews, E. H. Macromolecules 1997, 30, 2400.

29. Reynolds, N. M.; Hsu, S. L. Macromolecules 1990, 23, 78.

30. Gomez, M. A.; Tonelli, A. E. Macromolecules 1990, 23, 3385.

31. Licoln, D. M.; Vaia, R. A.; Wang, Z.-G.; Hsiao, B. S.; Krishnamoorti, R. Polymer 2001, 42, 9975.

32. VanderHart, D. L.; Asano, A.; Gilman, J. W. Chem Mater 2001, 13, 3781.

33. Strawhecker, K.; Manias, E. Chem Mater 2000, 12, 2943.

34. Strawhecker, K.; Manias, E. Macromolecules 2001, 34, 8475.

35. Sun, Y. S.; Woo, E. M. Macromolecules 1999, 32, 7836.

36. Hong, B. K.; Jo, W. H.; Lee, S. C.; Kim, J. Polymer 1998, 39, 1793.

37. Wu, H. D.; Wu. I. D.; Chang, F. C. Macromolecules 2000, 33, 8915.

38. Wang, Z.-M. M.Sc. Thesis, Penn State University, 2003.

39. Manias, E.; Touny, A.; Wu, L.; Strawhecker, K.; Lu, B.; Chung, T. C. Chem Mater 2001, 13, 3516.

40. Strawhecker, K.; Manias, E. Chem Mater 2003, 15, 844.

41. Strawhecker, K. Ph.D. Thesis, Penn State University, 2002.

42. Dong, J. Y.; Manias, E.; Chung, T. C. Macromolecules 2002, 35, 3439.